



Enhanced nodal gradient 3D consecutive-interpolation tetrahedral element (CTH4) for heat transfer analysis



Minh Ngoc Nguyen^a, Tinh Quoc Bui^{b,c,*}, Thien Tich Truong^a, Ngoc Anh Trinh^d, Indra Vir Singh^e, Tiantang Yu^f, Duc Hong Doan^{g,1}

^a Department of Engineering Mechanics, Faculty of Applied Sciences, Ho Chi Minh City University of Technology – Vietnam National University, Ho Chi Minh City, Viet Nam

^b Institute for Research and Development, Duy Tan University, Da Nang City, Viet Nam

^c Department of Civil and Environmental Engineering, Tokyo Institute of Technology, 2-12-1-W8-22, Ookayama, Meguro-ku, Tokyo, Japan

^d Department of Mechanics, Faculty of Mathematics and Computer Science, VNUHCM-University of Science, Viet Nam

^e Department of Mechanical and Industrial Engineering, Indian Institute of Technology Roorkee, Uttarakhand, India

^f Department of Engineering Mechanics, Hohai University, PR China

^g Department of Mechanical and Control Engineering, Tokyo Institute of Technology, Ookayama, Meguro-ku, Tokyo, Japan

ARTICLE INFO

Article history:

Received 12 May 2016

Received in revised form 6 July 2016

Accepted 12 July 2016

Keywords:

FEM

Tetrahedral element

Heat transfer

Consecutive-interpolation element

3D

ABSTRACT

In this paper, formulation of a novel consecutive-interpolation 4-node tetrahedral finite element (CTH4) and its applications to the analysis of heat transfer problems in three-dimension (3D) are presented. The field variables approximation is performed on the way of taking both the nodal values and their averaged nodal gradients into account, in terms of the consecutive-interpolation procedure (CIP). The new CTH4 element proposed inherently possesses many desirable advantages over the conventional tetrahedral element (TH4) such as the higher accuracy, higher-order continuity, and continuous nodal gradients without smoothing operation. Importantly, the number of degrees of freedom of the system does not change, but still remains the nodal values as that of the TH4 element. We demonstrate the accuracy and performance of the developed CTH4 element through a series of numerical experiments of 3D heat transfer problems, in which comparison between the present obtained results and reference solutions derived from analytical solutions and other numerical approaches is made. We additionally propose a general formulation of auxiliary functions in terms of the CIP method. As a result, a family of CIP-based elements in all dimensions (i.e., 1D up to 3D) can now straightforwardly be established since any auxiliary functions required by the CIP scheme are easily to be generated by using the present general formulation.

© 2016 Elsevier Ltd. All rights reserved.

1. Introduction

Heat transfer problems constitute a large class of engineering problems, and they present nearly in every activities, for example, the air-conditioning exploits the convection, both heat conduction and convection can be found in cooking, and the Earth receives heat from the Sun through thermal radiation. Due to a wide range of applications as these heat transfer problems span many engineering disciplines including aeronautical, electrical, mechanical and civil engineering etc. [1]. Therefore, analysis of heat transfer problems is of great importance to the scientific community. A

closed-form solution obtained by analytical approaches is currently only available for some specific problems with relatively simple geometry and boundary conditions. When it comes to deal with engineering problems which require modeling of more complicated geometries and/or boundary conditions, numerical approaches have shown to be more suitable.

Although the finite element method (FEM) has shown to be one of the most popular numerical methods in use nowadays, the method however inherently owns several shortcomings [1,2]. The FEM shape function is C^0 continuous, thus the nodal gradient fields, e.g., the temperature gradients in case of heat transfer problems, are discontinuous across element boundaries. The non-physical discontinuous gradient fields are required to be treated in post-processing.

Various alternatives have been previously proposed to investigate the heat transfer problems, such as the boundary element method (BEM) [3,4], the class of meshfree methods [5–8] and the smoothed finite element method [2], etc. Each method has its

* Corresponding author at: Institute for Research and Development, Duy Tan University, Da Nang City, Viet Nam.

E-mail addresses: buiquoctinh@duytan.edu.vn, tinh.buiquoc@gmail.com (T.Q. Bui).

¹ Current Address: Advanced Materials and Structures Laboratory, University of Engineering and Technology, Vietnam National University, Hanoi, 144 Xuan Thuy, Cau Giay, Hanoi, Viet Nam.

own advantages and disadvantages. For example, the BEM has shown advantages for some specific problems like crack modeling but it is not easy to extract the data at points inside the problem domain, and more importantly fundamental solutions for each specific problem are often required, which is not a trivial task for complex problems. The class of meshfree methods discretizes the problem domain into scattered nodes and consequently elements are no longer required, so that more flexibility is achievable when the domain or the discretization needs to be updated, such as in case of refinement or optimization. The smoothed finite element method employs mathematical smoothing operator to “smoothen” the nodal gradients.

The recent development of a consecutive-interpolation 4-node quadrilateral element (CQ4) for the analysis of mechanical stress of two-dimensional problems based on the consecutive-interpolation procedure (CIP) [9] was presented in [10]. Subsequently, the CQ4 has been extended to study transient problems of free and forced vibration for linear elastic and piezoelectric structures [11], and enhanced by enrichments for dealing with crack problems [12]. In this setting, the CQ4 element basis functions are constructed through two stages. The first stage is carried out the same interpolation functions as in the classical FEM for the 4-node quadrilateral element. The second stage is subsequently extended to include both the nodal values and the averaged values of gradients of the unknown function at the nodes [10,11]. The original goal proposed for the CIP is to improve the accuracy of the results and to smooth the stress fields in terms of FEM. In other words, the development of the CIP is to make the trial solution and its derivatives continuous across inter-element boundaries. The accuracy of the computed gradients of the trial solution should hence be improved and the smoothing techniques generally employed during the post-processing process should be avoided completely.

The conventional FEM approximations, which employ a linear combination of nodal values, are enhanced by adding other terms related to the averaged nodal gradients. As a consequence, the resulting shape functions that possess C^1 continuous across element boundaries are obtained and thus, the nodal gradient fields are continuous. Additional smoothness obtained by the CIP, in contrast to the conventional approximation, generally provides potential for higher-order accuracy because of solution regularity. In addition, the CQ4 shape functions possess the Kronecker- δ property, allowing directly imposition of essential boundary conditions. Furthermore, no additional degrees of freedom (DOFs) are required to the system and no modification is made to the finite element mesh. Hence, the unknowns remain the same as those of the FEM, which are the nodal values, and the same mesh as in FEM can be utilized.

From the practical applications point of view, there are only a few problems that could be simplified to 2D models. In most of the cases, researchers and engineers must deal with 3D problems, and developing effective numerical methods that are able to accurately simulate 3D problems is a natural demand. In the past few decades, many attempts have been devoted to the development of new or improved models for 3D thermal analysis. Both analytical [13,14] and numerical methods [5,15–18] are proposed, in order to provide higher accurate results and/or save computational time, which are well known as the two key criteria required in most practical applications. In particular industry-related problems, investigation often focuses on techniques that extends existing models in certain aspects. Gerace et al. [19] introduced a meshless-based procedure that allows automation from the discretization of problem domains, even with rather complicated geometry, to the output solution. This procedure is shown to significantly reduce the cost of computation, especially in solving

large-scale 3D problems. A quite popular and interesting application is the simulation of welding process, which includes moving heat source. Challenges in this application involves singularity due to very high temperature locally concentrated at the source and the necessity of fine mesh along the welding path. Relevant approaches such as adaptive addition and elimination of nodes within a meshless framework [20] and the partition of unity virtual node based on the polygonal finite element [21] have been developed. Recently, [22] developed a model for 3D transient heat analysis of a steel billet during the reheating process in steel industries, which enables the prediction of temperature field as well as the growth of oxidation on the billet surface. Another FEM based model to predict the temperature field in a power transformer bushing during working conditions was introduced by [23], providing insight information for manufacturers to evaluate insulation design and loss of insulation life within a power transformer.

Inspired by the advantages and potential of the consecutive-interpolation approach reported for the 2D linear elastic problems [9–12], in this paper we formulate for the first time a novel enhanced nodal gradient 4-node tetrahedral finite element (CTH4) based on the CIP for heat transfer analysis in 3D. The approximation for this new CTH4 element is performed on the way of taking both the nodal values and their averaged nodal gradients into account. Similarly, the proposed CTH4 element owns many advantages over the conventional tetrahedral element (TH4) such as the higher accuracy, higher-order continuity, and continuous nodal gradients without smoothing operation. Once again, importantly, the number of DOFs of the system does not change, but still remains the nodal values as that of the TH4 element.

In this paper, a general formulation that can be used for reproducing any auxiliary functions in terms of the CIP method is also proposed. Deriving this general formulation is indeed very important and useful in the development of the approach, where the auxiliary functions required for a class of CIP-based elements can now straightforwardly be derived. Here, the general form of the auxiliary functions will be derived, and some specific auxiliary functions for several CIP-based elements will be reproduced by using the new general formulation.

This paper is organized as follows. After the introduction, the formulation for the three-dimensional CTH4 element, which is based on the development of Consecutive-Interpolation procedure for the 4-node tetrahedral element Section 2, is presented in details. The weak form of heat transfer problems is shortly given in Section 3. Several numerical examples are investigated and discussed in Section 4. A general formulation of the auxiliary functions for the CIP approach is proposed in Section 5. Conclusions and outlooks are drawn in Section 6.

2. Formulation of consecutive-interpolation 4-node tetrahedral element (CTH4)

2.1. The consecutive-interpolation procedure (CIP)

Consider a general 3D body that occupies a domain $\Omega \in R^3$ and bounded by its boundary Γ . A function $u(\mathbf{x})$ is approximated through the consecutive-interpolation (CIP) scheme as [9–12]

$$u(\mathbf{x}) \approx \tilde{u}(\mathbf{x}) = \sum_{l=1}^n \left(\phi_l u^{[l]} + \phi_{lx} \bar{u}_x^{[l]} + \phi_{ly} \bar{u}_y^{[l]} + \phi_{lz} \bar{u}_z^{[l]} \right), \quad (1)$$

where n is the number of nodes and $u^{[l]}$ is the value of function $u(\mathbf{x})$ evaluated at node l by the finite element interpolation

$$u^{[l]} = u(\mathbf{x}_l) = \sum_{i=1}^n N_i \hat{u}_i = \mathbf{N} \hat{\mathbf{u}}. \quad (2)$$

The values $\bar{u}_x^{[I]}$, $\bar{u}_y^{[I]}$, and $\bar{u}_z^{[I]}$ are the averaged nodal gradient of $u(\mathbf{x})$ evaluated at node I . The first order derivative of $u_x^{[e]}(\mathbf{x}_I)$ evaluated at node I within an element e can be written by finite element interpolation as follows:

$$u_x^{[e]}(\mathbf{x}_I) = \sum_{l=1}^{ne} N_{I,x} \hat{u}_l = \mathbf{N}_x \hat{\mathbf{u}}, \quad (3)$$

with ne being the number of nodes within element e . After getting the nodal gradients $u_x^{[e]}(\mathbf{x}_I)$ for all the elements $e \in S_I$ that share the node I , the averaged value $\bar{u}_x^{[I]}$ can then be calculated using weighted averaging by

$$\bar{u}_x^{[I]} = \sum_{e \in S_I} \left(w_e \cdot \mathbf{N}_x^{[e]} \right) \hat{\mathbf{u}} = \bar{\mathbf{N}}_x \hat{\mathbf{u}}, \quad (4)$$

with the weights w_e defined by the ratio of the volume of element e and the total volume of the set S_I . The values $\bar{u}_y^{[I]}$ and $\bar{u}_z^{[I]}$ are computed in the same way.

In Eq. (1), the so-called auxiliary functions ϕ , $\phi_{I,x}$, $\phi_{I,y}$, $\phi_{I,z}$ have to be determined for each type of element and that must be satisfied the following conditions [9,10]

$$\begin{aligned} \phi_I(x_j) &= \delta_{IJ}, & \phi_{I,x}(x_j) &= 0, & \phi_{I,y}(x_j) &= 0, & \phi_{I,z}(x_j) &= 0 \\ \phi_{I,x}(x_j) &= 0, & \phi_{I,x,x}(x_j) &= \delta_{IJ}, & \phi_{I,x,y}(x_j) &= 0, & \phi_{I,x,z}(x_j) &= 0 \\ \phi_{I,y}(x_j) &= 0, & \phi_{I,y,x}(x_j) &= 0, & \phi_{I,y,y}(x_j) &= \delta_{IJ}, & \phi_{I,y,z}(x_j) &= 0 \\ \phi_{I,z}(x_j) &= 0, & \phi_{I,z,x}(x_j) &= 0, & \phi_{I,z,y}(x_j) &= 0, & \phi_{I,z,z}(x_j) &= \delta_{IJ} \end{aligned} \quad (5)$$

where J is any one of the indices i, j, k and m of the CTH4 element (which will subsequently be described in the following subsection), and

$$\delta_{IJ} = \begin{cases} 1 & \text{if } I=J \\ 0 & \text{it } I \neq J \end{cases} \quad (6)$$

These conditions are explained in [10]. The Eq. (1) can then be rewritten as

$$u(\mathbf{x}) \approx \tilde{u}(\mathbf{x}) = \sum_{l=1}^n R_l \hat{u}_l, \quad (7)$$

where the CIP shape function R_l associated with a node I is given by

$$R_I = \phi_I N_I + \phi_{I,x} \bar{N}_x^{[I]} + \phi_{I,y} \bar{N}_y^{[I]} + \phi_{I,z} \bar{N}_z^{[I]}. \quad (8)$$

For easily understanding the CIP concept, an illustration of the CIP scheme applied in a 2D domain is depicted in Fig. 1 [10]. Assume that the point of interest \mathbf{x} is located inside a 4-node quadrilateral element, where the 4 nodes are denoted as i, j, k, m . Firstly, nodal values and the nodal gradients are evaluated using the standard finite element procedure. Then the four sets S_i, S_j, S_k, S_m containing the elements that share the node i, j, k, m , respectively, have to be determined. Once the sets S_i, S_j, S_k, S_m are found, the weighted average of the nodal gradients can be computed. It is noted from Fig. 1 that the support domain of a point of interest \mathbf{x} is in general larger than that in the conventional FEM. The nodes that support the point \mathbf{x} include all the nodes in the element sets S_i, S_j, S_k, S_m , whereas in the classical FEM, the supporting nodes are simply the four nodes i, j, k, m . The application of CIP scheme for a 3D domain is quite similar.

2.2. Formulation of novel consecutive-interpolation 4-node tetrahedral element (CTH4)

The formulation of the new consecutive-interpolation 4-node tetrahedral element (CTH4) is presented here in this section. To this end, we apply the CIP scheme to a 4-node tetrahedral element. A schematic sketch of the tetrahedral element in physical coordinates and its mapping in natural coordinates is represented in Fig. 2. Illustration of support domain of a CTH4 element is sketched on Fig. 3 (Note: the rest of the mesh is omitted for the sake of clarity). We denote four nodes by i, j, k, m , and consequently the four shape functions associated with these nodes are given by

$$L_i = 1 - \xi - \eta - \zeta \quad (9)$$

$$L_j = \xi \quad (10)$$

$$L_k = \eta \quad (11)$$

$$L_m = \zeta \quad (12)$$

The partial derivatives can then be calculated by

$$\begin{bmatrix} \frac{\partial}{\partial x} \\ \frac{\partial}{\partial y} \\ \frac{\partial}{\partial z} \end{bmatrix} = \mathbf{J}^{-1} \begin{bmatrix} \frac{\partial}{\partial \xi} \\ \frac{\partial}{\partial \eta} \\ \frac{\partial}{\partial \zeta} \end{bmatrix}, \quad (13)$$

where the Jacobian matrix is computed as follows:

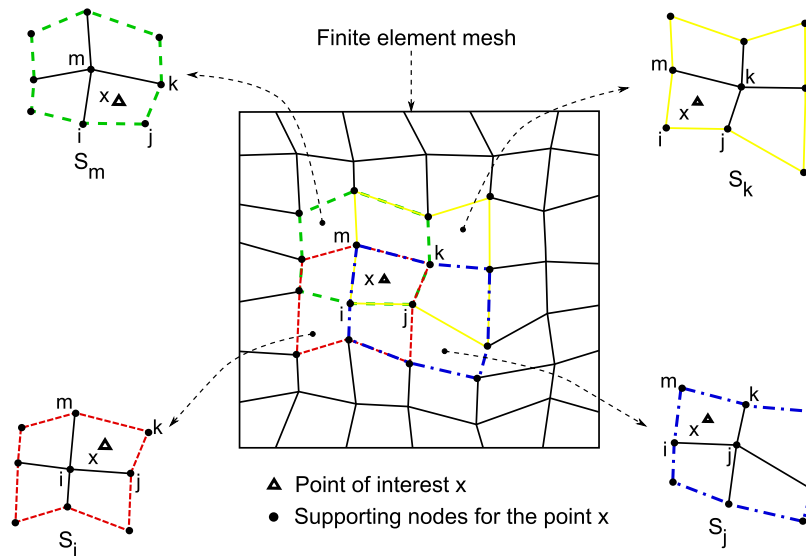


Fig. 1. Sketch of the CIP approach on a 4-node quadrilateral element [10].

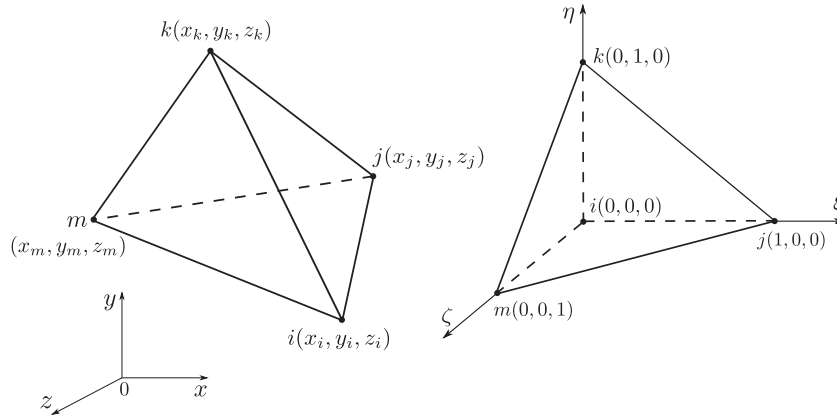


Fig. 2. Sketch of a 4-node tetrahedral element in physical space (left-hand) and in natural space (right-hand).

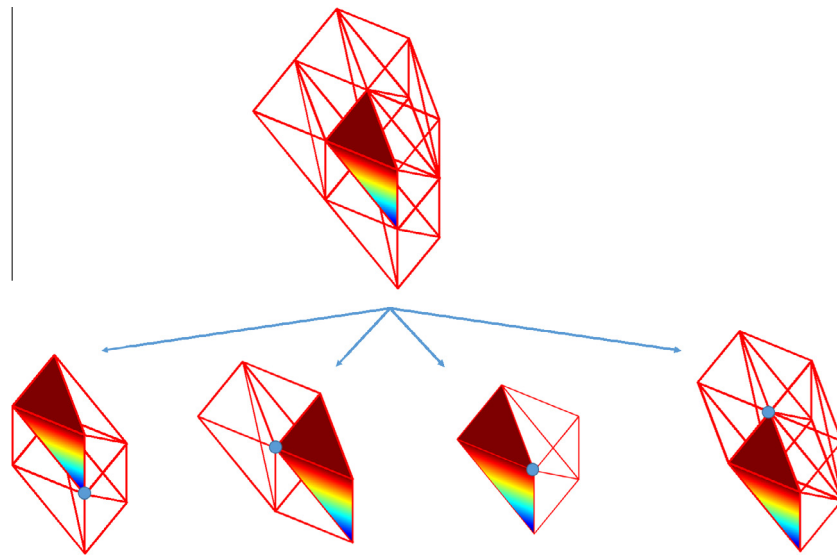


Fig. 3. Schematic representation of the support domain for a CTH4 element. Similar to the CQ4 element [10], the support domain of the proposed CTH4 element is in general larger than that of the traditional TH4 because of the CIP scheme, by adding extra nodes from its neighboring elements into the interpolation procedure. Consequently, the bandwidth of the so-called B-matrix (see Section 3) in terms of the CIP method is larger than that of the non-CIP one. In other words, the number of the supporting nodes, generally $n > 4$. Curious readers can find more information regarding this issue as it is already discussed in [10–12] or [9].

$$\mathbf{J} = \begin{bmatrix} \frac{\partial x}{\partial \xi} & \frac{\partial y}{\partial \xi} & \frac{\partial z}{\partial \xi} \\ \frac{\partial x}{\partial \eta} & \frac{\partial y}{\partial \eta} & \frac{\partial z}{\partial \eta} \\ \frac{\partial x}{\partial \zeta} & \frac{\partial y}{\partial \zeta} & \frac{\partial z}{\partial \zeta} \end{bmatrix} = \begin{bmatrix} \frac{\partial L_i}{\partial \xi} & \frac{\partial L_j}{\partial \xi} & \frac{\partial L_k}{\partial \xi} & \frac{\partial L_m}{\partial \xi} \\ \frac{\partial L_i}{\partial \eta} & \frac{\partial L_j}{\partial \eta} & \frac{\partial L_k}{\partial \eta} & \frac{\partial L_m}{\partial \eta} \\ \frac{\partial L_i}{\partial \zeta} & \frac{\partial L_j}{\partial \zeta} & \frac{\partial L_k}{\partial \zeta} & \frac{\partial L_m}{\partial \zeta} \end{bmatrix} \begin{bmatrix} x_i & y_i & z_i \\ x_j & y_j & z_j \\ x_k & y_k & z_k \\ x_m & y_m & z_m \end{bmatrix}, \quad (14)$$

The functions $\phi_i, \phi_{ix}, \phi_{iy}$ and ϕ_{iz} are given by

$$\phi_i = L_i + L_i^2(L_j + L_k + L_m) - L_i(L_j^2 + L_k^2 + L_m^2) \quad (15)$$

$$\begin{aligned} \phi_{ix} = & -(x_i - x_j)(L_i^2 L_j + pL_i L_j L_k + pL_i L_j L_m) \\ & - (x_i - x_k)(L_i^2 L_k + pL_i L_k L_m + pL_i L_k L_j), \\ & - (x_i - x_m)(L_i^2 L_m + pL_i L_m L_j + pL_i L_m L_k) \end{aligned} \quad (16)$$

$$\begin{aligned} \phi_{iy} = & -(y_i - y_j)(L_i^2 L_j + pL_i L_j L_k + pL_i L_j L_m) \\ & - (y_i - y_k)(L_i^2 L_k + pL_i L_k L_m + pL_i L_k L_j), \\ & - (y_i - y_m)(L_i^2 L_m + pL_i L_m L_j + pL_i L_m L_k) \end{aligned} \quad (17)$$

$$\begin{aligned} \phi_{iz} = & -(z_i - z_j)(L_i^2 L_j + pL_i L_j L_k + pL_i L_j L_m) \\ & - (z_i - z_k)(L_i^2 L_k + pL_i L_k L_m + pL_i L_k L_j), \\ & - (z_i - z_m)(L_i^2 L_m + pL_i L_m L_j + pL_i L_m L_k) \end{aligned} \quad (18)$$

with $p = 0.5$. The functions $\phi_j, \phi_{jx}, \phi_{jy}, \phi_{jz}; \phi_k, \phi_{kx}, \phi_{ky}, \phi_{kz}; \phi_m, \phi_{mx}, \phi_{my}, \phi_{mz}$ can be computed similarly by a cyclic permutation of the indices i, j, k, m .

2.3. Modification to retain the C^0 -continuity

The formulation of Consecutive-interpolation scheme leads to elements that can reproduce continuous nodal gradients. In cases where the C^0 -continuity at node is necessary, such as on material interfaces and geometrical boundaries, it is required to modify the formulation, such that the “nodal averaged gradient” is replaced by nodal gradient, i.e., [9,10]

$$\bar{u}_x^{[i]} = u_x^{[e]}. \quad (19)$$

By this slight modification, C^0 -continuity can be recovered for any given nodes. In fact, if the modification is applied to all the nodes in the problem domain, the CIP based elements will degenerate to the standard FEM.

3. Weak form of heat transfer problem

The governing equation of a heat transfer problem is given by

$$\nabla \cdot (\mathbf{k}\nabla T) + Q = \rho c_p \frac{\partial T}{\partial t}, \tag{20}$$

with the following boundary conditions

$$T = \bar{T}, \text{ on } \Gamma_1 : \text{ Dirichlet boundary} \tag{21}$$

$$(\mathbf{k}\nabla T) \cdot \mathbf{n} = \bar{q}, \text{ on } \Gamma_2 : \text{ Neumann boundary} \tag{22}$$

$$(\mathbf{k}\nabla T) \cdot \mathbf{n} = h(T_a - T), \text{ on } \Gamma_3 : \text{ convection boundary} \tag{23}$$

$$(\mathbf{k}\nabla T) \cdot \mathbf{n} = \varepsilon\sigma(T_a^4 - T^4), \text{ on } \Gamma_4 : \text{ radiation boundary.} \tag{24}$$

In Eq. (20), $\mathbf{k} = \text{diag}(k_{xx}, k_{yy}, k_{zz})$ is the tensor of thermal conductivities, T the temperature, Q the heat sink/source, ρ the density and c_p the specific heat capacity. In the boundary conditions Eqs. (21)–(24), \bar{T} is the prescribed temperature, \bar{q} the prescribed heat flux, \mathbf{n} the normal vector pointing outward of the boundary, T_a the ambient temperature, ε the emissivity and σ the Stefan-Boltzmann constant for radiation.

The weak form of heat transfer problem is obtained by multiplying both sides of Eq. (20) with a test function δT and integrating over the entire domain

$$\int_{\Omega} \nabla \cdot (\mathbf{k}\nabla T) \delta T d\Omega + \int_{\Omega} Q \delta T d\Omega = \int_{\Omega} \rho c_p \frac{\partial T}{\partial t} \delta T d\Omega, \tag{25}$$

Integration by parts and apply the Gauss theorem, yield

$$\begin{aligned} & \int_{\Omega} \rho c_p \frac{\partial T}{\partial t} \delta T d\Omega + \int_{\Omega} (\delta \nabla T) \mathbf{k} \nabla T d\Omega \\ & - \int_{\Gamma} (\delta T) (\mathbf{k} \nabla T) \cdot \mathbf{n} d\Gamma - \int_{\Omega} Q \delta T d\Omega = 0, \end{aligned} \tag{26}$$

and applying the boundary conditions, the following equation is obtained

$$\begin{aligned} & \int_{\Omega} \rho c_p \frac{\partial T}{\partial t} \delta T d\Omega + \int_{\Omega} (\delta \nabla T) \mathbf{k} \nabla T d\Omega - \int_{\Omega} Q \delta T d\Omega \\ & - \int_{\Gamma} \bar{q} \delta T d\Gamma - \int_{\Gamma} h(T_a - T) \delta T d\Gamma - \int_{\Gamma} \varepsilon\sigma(T_a^4 - T^4) \delta T d\Gamma = 0, \end{aligned} \tag{27}$$

After the temperature field is determined, the thermal energy over the whole domain is calculated through

$$\Psi = \left(\int_{\Omega} \mathbf{B}^T \mathbf{k} \mathbf{B} d\Omega \right) \hat{\mathbf{T}}, \tag{28}$$

where $\hat{\mathbf{T}}$ is the nodal temperature values and \mathbf{B} is the matrix of the derivatives of shape functions

$$\mathbf{B} = \begin{Bmatrix} \frac{\partial R_1}{\partial x} & \frac{\partial R_2}{\partial x} & \dots & \frac{\partial R_n}{\partial x} \\ \frac{\partial R_1}{\partial y} & \frac{\partial R_2}{\partial y} & \dots & \frac{\partial R_n}{\partial y} \\ \frac{\partial R_1}{\partial z} & \frac{\partial R_2}{\partial z} & \dots & \frac{\partial R_n}{\partial z} \end{Bmatrix} \tag{29}$$

Remark 1. It is worth stressing out that the effects of the numerical integration on the accuracy of the solution in terms of CIP have already been analyzed and presented in [10,11] for both static and dynamic problems. Since no special methods are required for the numerical integration of the CIP. Any quadrature

rules used for the conventional FEM can be applied the same for the CIP. Higher number of quadrature points does not influence too much on the accuracy of the results. Here throughout the analysis we merely adopt 3 quadrature points for both T3/CT3 (2D numerical examples) and 4 quadrature points for both TH4/CTH4 (3D numerical examples).

4. Numerical results and discussions

In this section, the new CTH4 element is applied to solve some numerical examples of heat transfer problems in 3D and the obtained results are then presented and discussed in detail. To validate the accuracy of the proposed CTH4 element, the numerical results computed are therefore compared with reference solutions derived from, for instance, analytical solutions [24], the meshless CS-RPIM [8], and the conventional TH4 element. The first two numerical examples deal with heat transfer problems in 2D with exact solutions, while the other four numerical examples devoted to 3D heat transfer problems. Notice that the temperature field considered throughout the study is set to be either in °C or in K, which is depended upon each example.

In this numerical results section, the following elements are used:

- CT3: the CIP-based 3-node triangular element [9].
- TH4: the standard 4-node tetrahedral element.
- CTH4: the proposed CIP-based 4-node tetrahedral element.

4.1. A square plate with Dirichlet conditions

We start showing the accuracy and applicability of CIP based finite elements in modeling heat transfer problems by considering numerical examples in 2D, with which analytical solutions are available. We first consider a steady-state heat conduction in a square domain $L \times L$ as shown in Fig. 4. The temperature on the top side is prescribed as $T = \sin(\frac{\pi x}{L})$, whereas the other sides are kept to be constant, i.e., $T = 0^\circ\text{C}$. The thermal conductivity is given

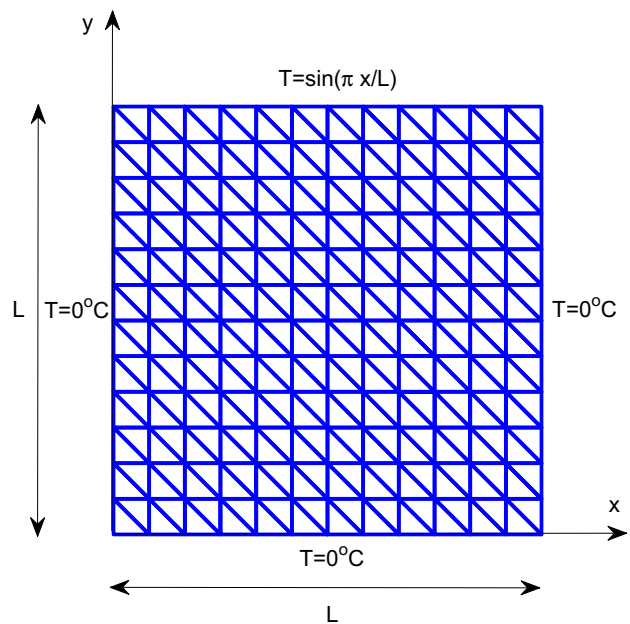


Fig. 4. Example 4.1. Geometry and finite element mesh of a square plate with Dirichlet condition.

by $k = 10 \text{ W/m}^\circ\text{C}$. The analytical solution for this particular problem can be found in [24] as follows:

$$T = \frac{\sinh(\pi y/L)}{\sinh(\pi)} \sin\left(\frac{\pi x}{L}\right). \quad (30)$$

This 2D problem is solved using a structured mesh of 288 CT3 elements [9,10] as shown in Fig. 4. The temperature field is displayed in Fig. 5. A comparison of temperature along the horizontal lines $y = 3L/4, y = L/2$ and $y = L/4$ obtained by CT3 element and analytical solution is depicted in Fig. 6. It can be observed from the given results that the CT3 offers a very good solution as its temperature values match well that of the exact values, revealing the high accuracy of the CT3 element. Fig. 7 shows the heat flux in x -direction, demonstrating that the gradient field obtained by CIP approach is continuous.

We study the convergence and error properties of the continuity of gradient across the element edges. The gradient field, which is the heat flux or thermal flux in this numerical example, is taken into account. The convergence property is carried out for both the conventional T3 and CT3 elements. Three different meshes such as $4 \times 4, 7 \times 7$ and 13×13 nodes are considered. The heat flux in x -direction along the edge, e.g., $x = L/3$, at all nodes, which involve the primary discretized nodes and new middle nodes, are measured. In other words, the heat flux at the middle nodes across the two element edges is estimated for three different given meshes respectively, and their corresponding averaged values are then obtained. The error norm for the numerical results of heat flux estimated over analytical solutions is computed. Fig. 8 shows the convergence rate of the error norm of the heat flux in x -direction against the total number of DOFs calculated for both the T3 and CT3 elements. It is indicated that the CT3 performs better than the standard T3 in terms of the continuity of the gradient (heat flux) across the element edges.

4.2. Transient heat transfer in a square domain

Next, the transient heat conduction in a square domain $\pi\text{m} \times \pi\text{m}$ is investigated. The configuration parameters of this square domain is taken the same as that considered in the previous example, see Fig. 4, but zero temperature, $T = 0^\circ\text{C}$, are imposed on all the sides of the problem domain instead. The initial temperature on the whole domain is given by [25]. Notice in Fig. 4 where L is taken to be π in this analysis.

$$T(x, y, 0) = 10 \sin(x) \sin(y). \quad (31)$$

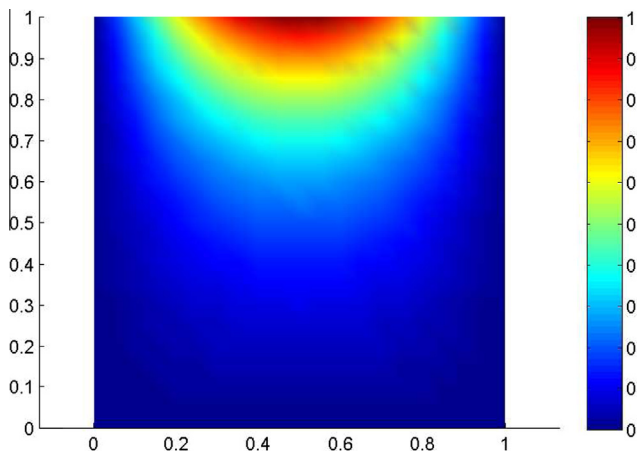


Fig. 5. Example 4.1. Distribution of the temperature ($^\circ\text{C}$) in a square plate with Dirichlet condition obtained by the CT3 element.

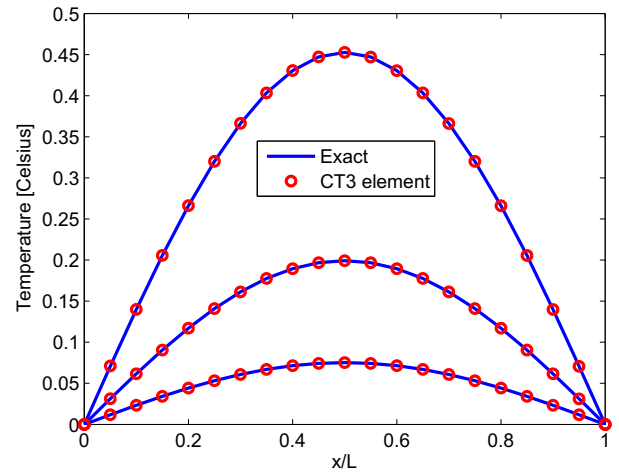


Fig. 6. Example 4.1. Comparison of temperature values along the line $y = L/4, y = L/2$ and $y = 3L/4$ between the CT3 and the exact solution.

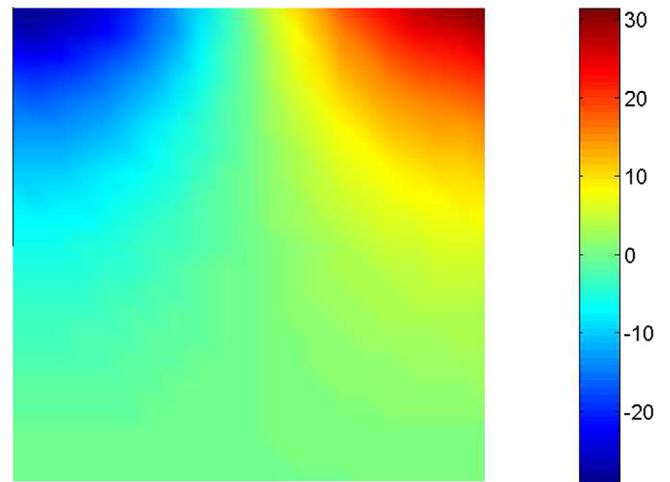


Fig. 7. Example 4.1. Heat flux (W/m^2) in x -direction of a square plate with Dirichlet condition obtained by the CT3 element.

The material parameters used for this particular example are given as follows: the mass density $\rho = 1 \text{ kg/m}^3$, the specific heat $c = 1 \text{ J/kg}^\circ\text{C}$, and the heat conductivity $k = 1 \text{ W/m}^\circ\text{C}$. With the geometry and boundary conditions as mentioned above, the temperature tends to drop down from the initial value to zero. The analytical solution of this problem is available in [25] and can be written by

$$T(x, y, t) = 10 \sin(x) \sin(y) e^{-2t}. \quad (32)$$

The transient solution is obtained numerically for the first 3 s (150 steps), by also using the same number of elements as that accounted for the previous example, i.e., 288 CT3 elements. For this example, the backward Euler time integration is used. Fig. 9 depicts the variation of temperature with respect to time, estimated at specific locations, e.g., point A $(\frac{\pi}{4}, \frac{\pi}{4})$ and point B $(\frac{\pi}{2}, \frac{\pi}{2})$. The gained results computed by the CT3 element match well with the analytical solution. The temperature decreases with increasing the time.

Remark 2. We notice that the consistent mass has been studied in our recent work, see e.g., [11] for 2D structural dynamic analysis. The nodal mass matrix is calculated exactly in the same way as that the conventional FEM does. No special methods are required. However, the only difference is its support domain, which is found

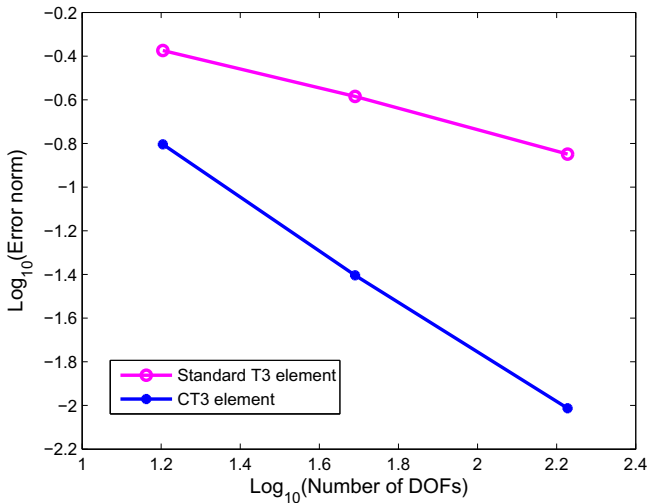


Fig. 8. Example 4.1. Convergence rate of the error norm of heat flux (W/m^2) across the element edges in x-direction of a square plate with Dirichlet condition versus the total number of DOFs for both the standard T3 and the CT3 elements. It shows that the CT3 significantly performs better than the T3 in terms of the continuity of the gradient across the element edges.

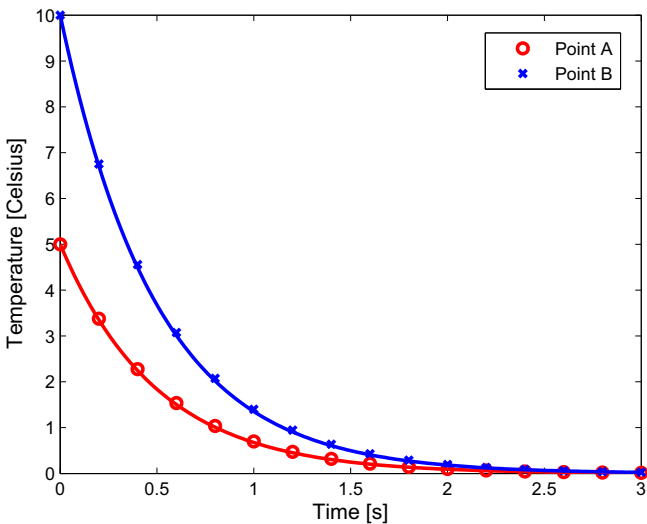


Fig. 9. Example 4.2. Comparison of temperature calculated at point A ($(\frac{\pi}{4}, \frac{\pi}{4})$) and point B ($(\frac{\pi}{2}, \frac{\pi}{2})$) between analytical solution (solid lines) and CT3 element (symbols).

to be larger than that of the FEM due to the CIP (through the CIP shape function). As usual, the nodal mass matrix for the thermal system, explicit form can be found in [25], is calculated in such a way.

4.3. A simple 3D heat conduction

Next numerical example deals with a simple 3D heat conduction whose geometry and boundary conditions are shown in Fig. 10 [2]. The inward heat flux on the top surface is set to be $q = 8000 W/m^2$. The temperature on bottom surface is prescribed as $T = 293 K$, while the heat conductivity is $k = 200 W/mK$. An insulated boundary condition is set for other faces.

The CTH4 element is applied to solve this simple 3D heat conduction. A coarse unstructured mesh of 1691 tetrahedral elements is typically shown in Fig. 11. The temperature field obtained by this mesh using CTH4 element is depicted in Fig. 12. Fig. 13 shows the convergence of the thermal energy with respect to the number of

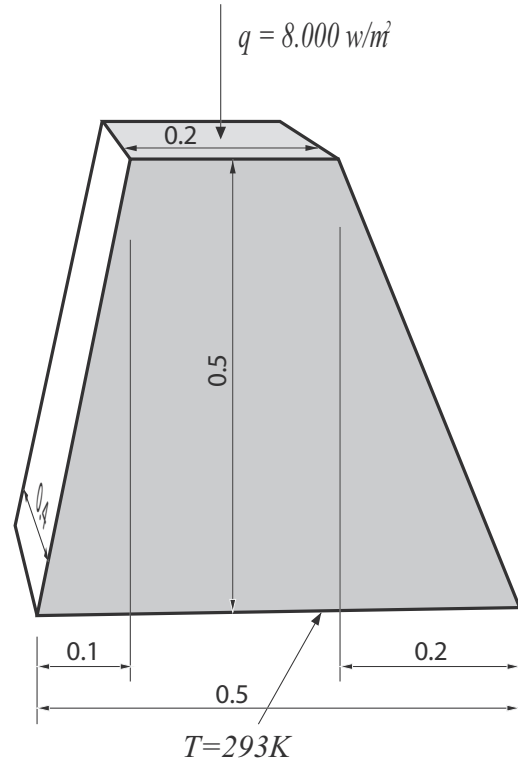


Fig. 10. Example 4.3. Geometrical representation and boundary conditions of a simple 3D heat conduction.

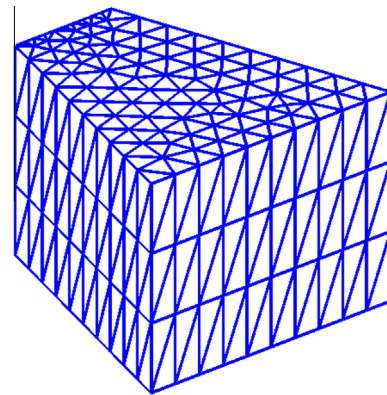


Fig. 11. Example 4.3. A typical finite element mesh of 1691 tetrahedral elements of a simple 3D heat conduction.

degrees of freedom (DOFs). It is observed that the CTH4 element provides an upper bound solution while a lower bound one is obtained by the TH4 element. The thermal energy calculated by CTH4 converges to the reference solution faster than the FEM counterpart. Here, due to the unavailability of the analytical solution, reference result is derived from numerical result using a very fine mesh FEM with 59594 TH4 elements (12298 DOFs). The comparison on the convergence rate of the proposed CTH4 element and the standard tetrahedral element (TH4) is additionally depicted in Fig. 14, where the relative error is determined by

$$\epsilon = \frac{|u_{num} - u_{ref}|}{|u_{ref}|}, \tag{33}$$

in which u_{ref} the reference value and u_{num} the computational value. A comparison of the heat flux, i.e., the temperature gradient field $-k \frac{\partial T}{\partial y}$ is shown in Fig. 15. It is apparently the gradient field

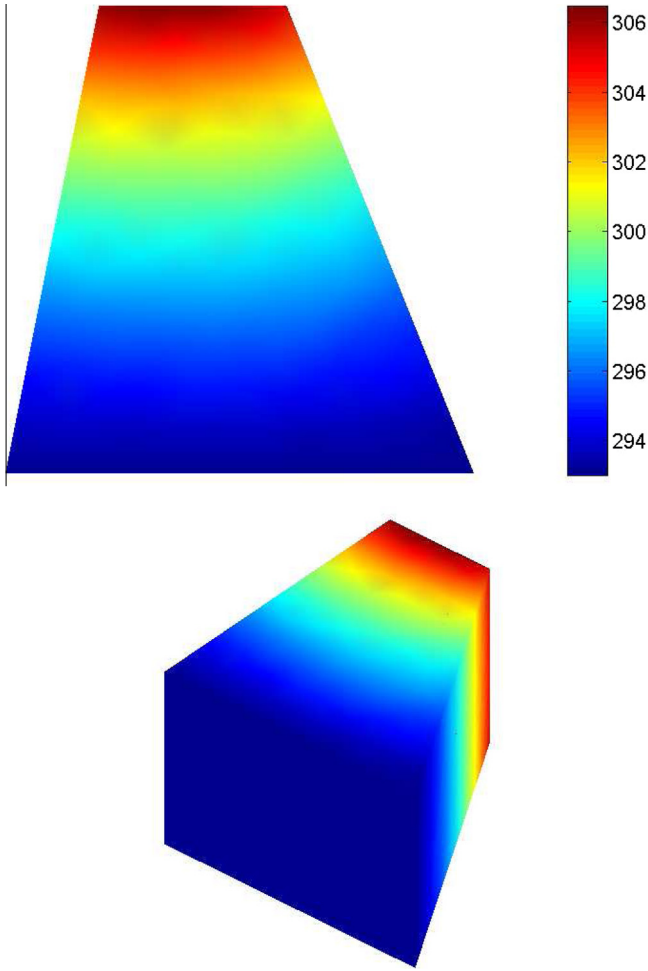


Fig. 12. Example 4.3. Temperature distribution on x - y plane view (upper) and 3D view (lower) obtained by the developed CTH4 element.

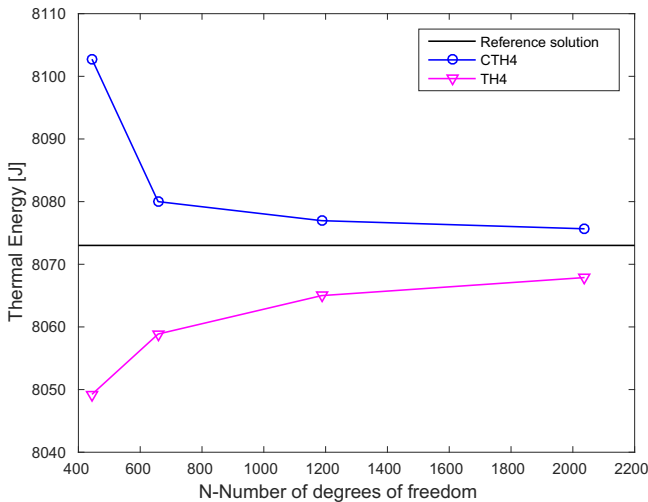


Fig. 13. Example 4.3. Convergence of the thermal energy of a simple 3D heat conduction obtained by CTH4 and TH4 elements. The reference solution is the numerical result derived from the TH4 with a very fine mesh.

obtained by the developed CTH4 element is smooth, which is not found in the results derived from the conventional TH4 element. In fact, the smoothness of the temperature gradient field delivered by the CTH4 is one of the main advantages of the CIP based

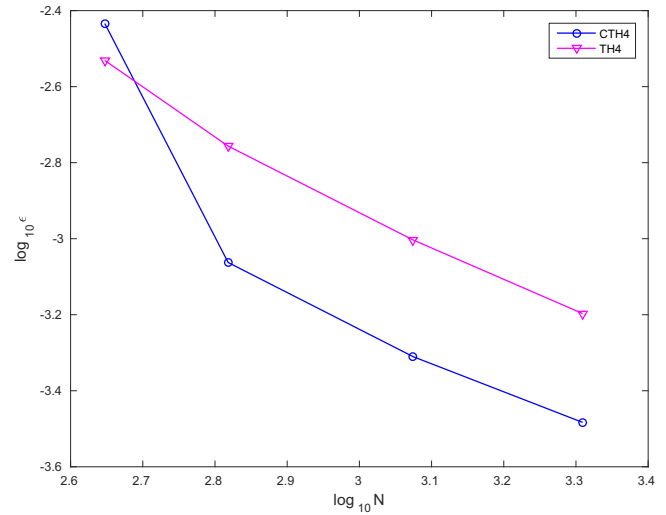


Fig. 14. Example 4.3. Comparison of the convergence rate of thermal energy in CTH4 and TH4 element. (N: number of DOFs, ϵ : relative error or thermal energy).

approaches, where the smoothing operator in post-processing required in the classical FEM is no longer a mandatory task.

Additional comment is concerned with the work done by Li et al. [2] using the so-called hybrid smoothed finite element method (HS-FEM), where this example was investigated. Unlike the HS-FEM in which a smoothed operator is applied to the gradient field such that the derivative operator has to be modified, the CIP under consideration does not require any smoothed operators. Furthermore, another difficulty of the HS-FEM is the parameter α [2], which has to be determined differently for each mesh size, and the parameter may be problem-dependent. Also, as reported in [2], such parameter α has a significant effect on the thermal energy. They show that the effect is reduced only when the mesh is fine enough. There is, however, no additional parameter in the CIP based elements, which could make the developed CTH4 element dominates over the HS-FEM in this particular heat transfer analysis. Curious readers must be noted that we are only able to give some comments here between two approaches, and no appropriate comparison of the outputs between the CTH4 and the HS-FEM is made since no given results reported in [2] are suitable to be compared with.

4.4. Heat convection in a 3D complicated domain

Inspired by the work reported in [2] dealing with the heat transfer in a 2D heat sink, here the problem is extended to 3D space by extruding the geometry with a depth of 0.05, which is shown in Fig. 16. The main goal of solving this example is to demonstrate the applicability of the new CTH4 element in modeling heat transfer problems in 3D complicated geometry. To this end, the conductivity for this example is set to be $k = 100 \text{ W/mK}$. The inward heat flux is defined on the curved surface of the middle fin with a value of $q = 20,000 \text{ W/m}^2$. The Robin boundary condition is applied on the left hand side surface ($x = 0$) with an ambient temperature of $T_a = 300 \text{ K}$ and a convective coefficient of $h = 100 \text{ W/m}^2$. The Dirichlet boundary condition is prescribed as $T = 300 \text{ K}$ on the right hand side surface ($x = 0.5$).

The numerical analysis is first carried out using a coarse unstructured mesh of 3689 tetrahedral elements as shown in Fig. 17. Fig. 18 depicts the distribution of temperature field, showing that the maximum value on the Neuman boundary is found, and the minimum one is on the Robin boundary. A comparison of the maximum temperature obtained by the TH4 and CTH4

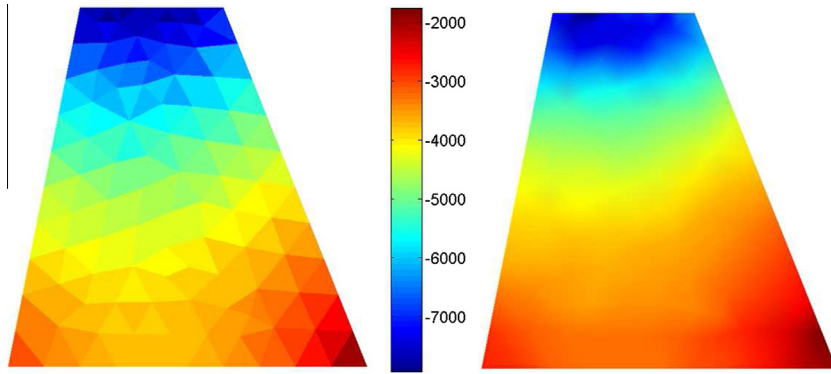


Fig. 15. Example 4.3. Comparison of heat flux in y-direction between TH4 (left-hand) and CTH4 element (right-hand) with the same mesh of 1691 tetrahedral elements. One must pay attention that the developed CTH4 element (right-hand) offers smoother heat flux field than that of the conventional TH4 element (left-hand).

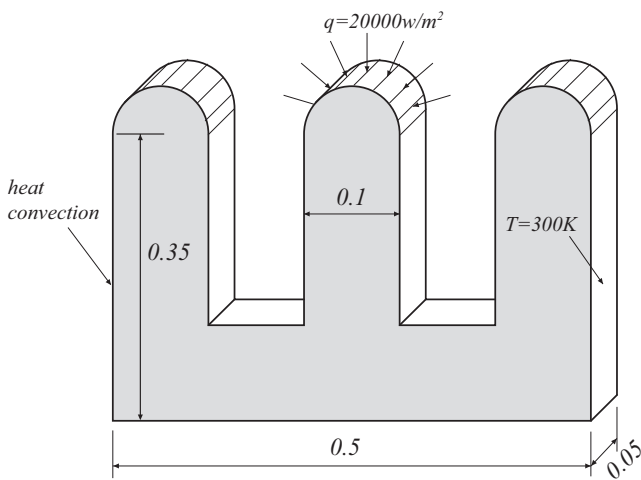


Fig. 16. Example 4.4. Geometrical representation and boundary conditions of a 3D heat sink.

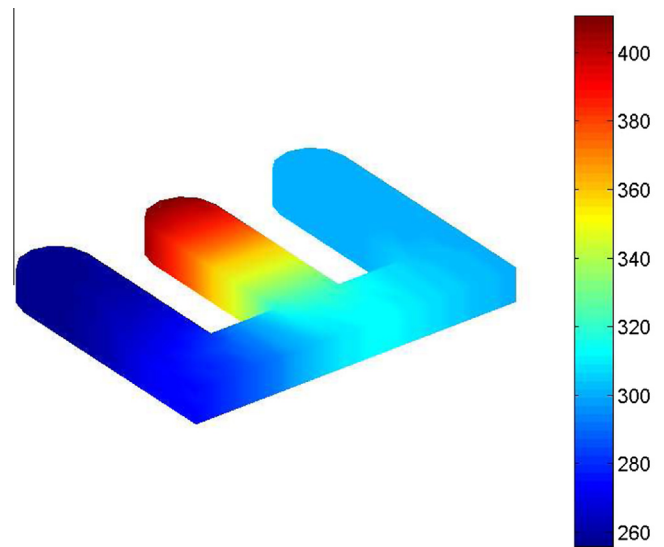


Fig. 18. Example 4.4. Temperature distribution in a 3D heat sink obtained by the developed CTH4 element.

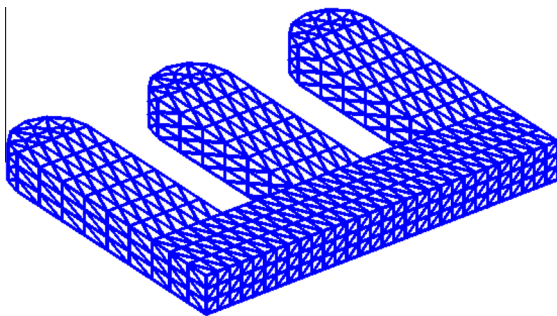


Fig. 17. Example 4.4. A coarse mesh of 3689 tetrahedral elements of a 3D heat sink.

elements is illustrated in Fig. 19 with various meshes, exhibiting higher accuracy of the CTH4 solution over the conventional TH4 results. One must be noted that the results of the TH4 and CTH4 visualized in Fig. 19 are calculated using the same meshes. Due to the lack of analytical solutions, and for the comparison purpose we herein again derive a reference solution which is carried out using the TH4 element but with a very fine mesh of 83925 tetrahedral elements (17668 DOFs). Fig. 20 shows that the convergence rate by the proposed CTH4 element is faster than that in the TH4. The nodal gradient temperature is also plotted in Fig. 21, where it is again observed that, as expected, the CTH4 result is smoother than the FEM solution.

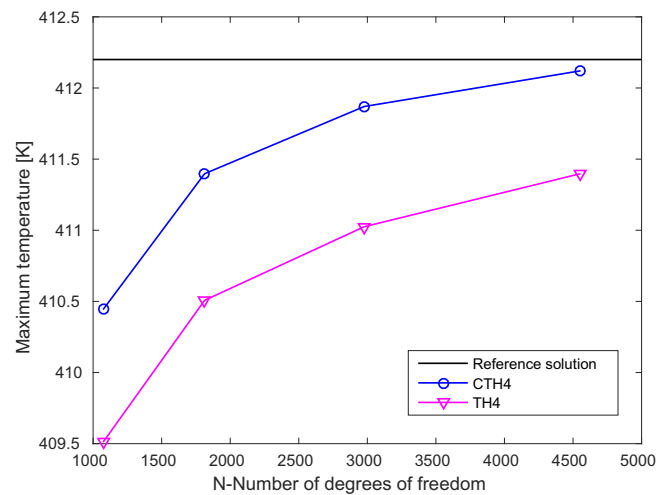


Fig. 19. Example 4.4. Convergence of the maximum temperature of the CTH4 and TH4 element with various meshes for a 3D heat sink problem. The reference solution is the numerical result derived from the TH4 with a very fine mesh.

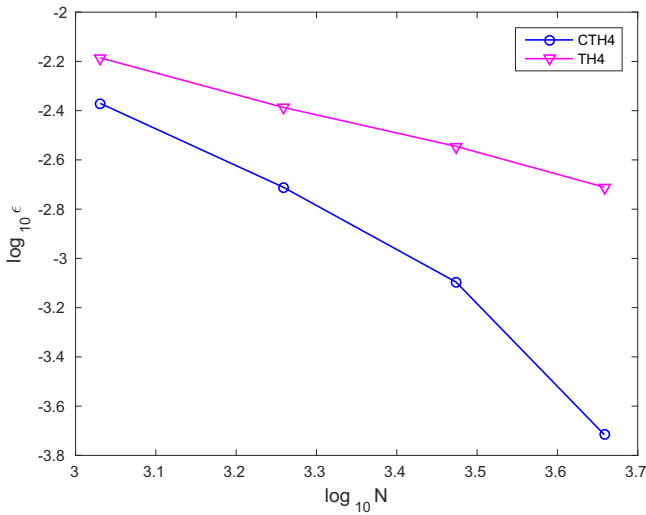


Fig. 20. Example 4.4. Comparison of the convergence rate of maximum temperature of a 3D heat sink problem between the CTH4 and TH4 elements.

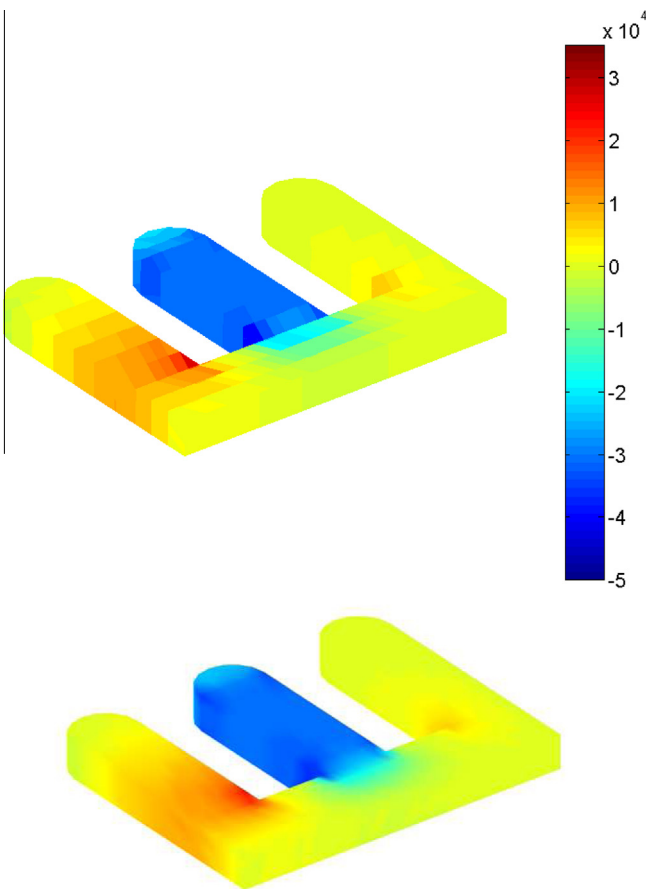


Fig. 21. Example 4.4. Comparison of the y-component of the nodal heat flux obtained by the TH4 element (upper) and the CTH4 element (lower). The discontinuity of the heat flux can be found in the TH4 result, whereas smooth result is obtained for the CTH4 element.

4.5. A square plate with a cylindrical hole

The next numerical example is concerned with the analysis of transient heat transfer problem of a square plate with a cylindrical hole at center. The plate is subjected to both Robin and Dirichlet

boundary conditions as shown in Fig. 22. Due to the geometrical symmetry, only a quarter of the plate is taken into account. The material parameters for this example are taken as follows: the conductivity $k_x = k_y = k_z = 15 \text{ W/m}^\circ\text{C}$, the convective coefficient is $h = 200 \text{ W/m}^2 \text{ }^\circ\text{C}$, the density is $\rho = 7800 \text{ kg m}^{-3}$ and the specific heat capacitance is $c = 125 \text{ J/kg }^\circ\text{C}$. Initially, the temperature of the entire domain is set to be $T_0 = 50 \text{ }^\circ\text{C}$. The prescribed temperature on the Dirichlet boundary is imposed by $\bar{T} = 200 \text{ }^\circ\text{C}$. For the Robin condition, an ambient temperature is set by $T_a = 100 \text{ }^\circ\text{C}$. The goal of the numerical simulation is to evaluate the heat transfer within a duration of 750 s, which is, as shown by the results, long enough to get steady state solution. A finite element mesh of 1728 tetrahedral elements is depicted in Fig. 23.

Fig. 24 sketches the steady-state distribution of temperature obtained by the developed CTH4 element. The evolution of temperature at point A (coordinate (0.1, 0.1, 0.02), see Fig. 22) in terms of time is shown in Fig. 25. It is observed that the gained result agrees well with the CS-RPIM solution reported in [8], though the CTH4 result tends to be higher than its CS-RPIM counterpart. The convergence of the steady-state temperature at point A obtained by the CTH4 element is depicted in Fig. 26, where the reference data is calculated by a fine mesh FEM (110575 tetrahedral elements). Even with a coarse mesh, the CTH4 result (138 °C) only has a small relative error, compared to the reference data (138.505 °C), i.e., -0.365%. The CTH4 result using the coarse mesh is also in good

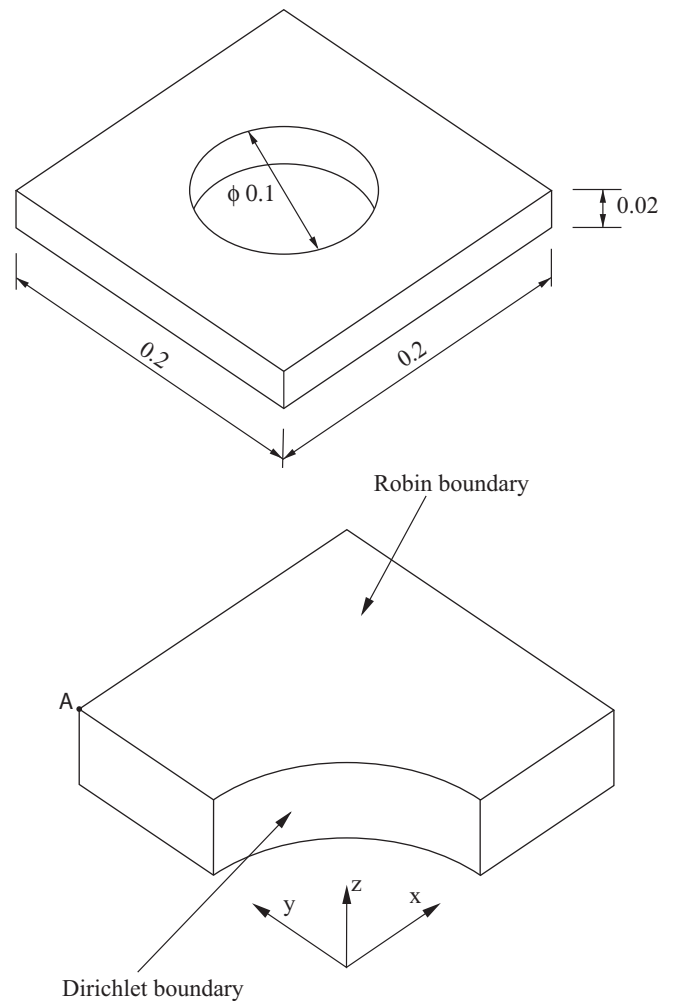


Fig. 22. Example 4.5. Geometry and dimension of the square plate with a cylindrical hole (upper), and its quarter model (lower).

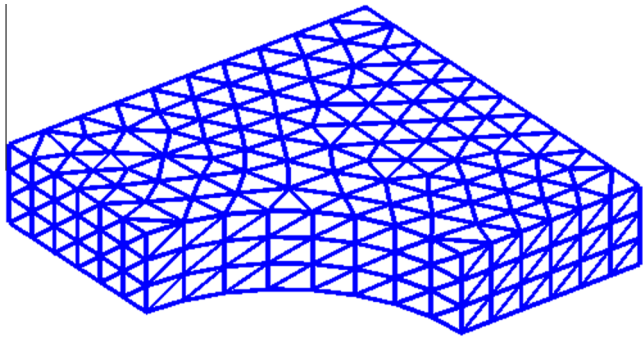


Fig. 23. Example 4.5. A coarse mesh of 1728 tetrahedral elements discretized for a quarter of the square plate with a cylindrical hole.

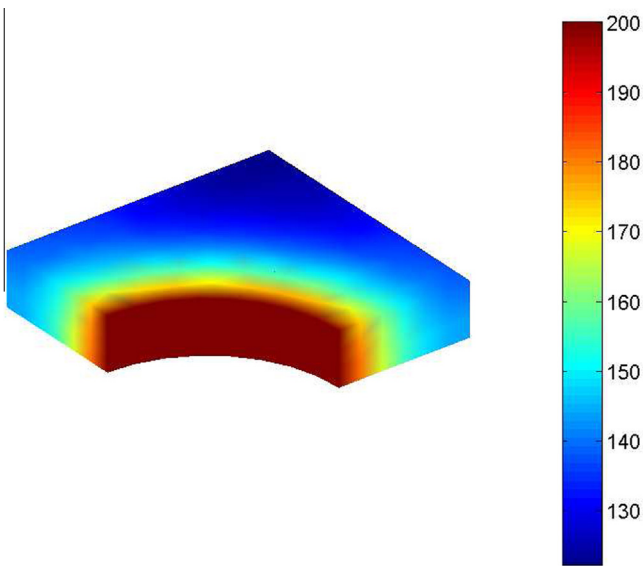


Fig. 24. Example 4.5. Distribution of temperature in a quarter of a square plate with a cylindrical hole.

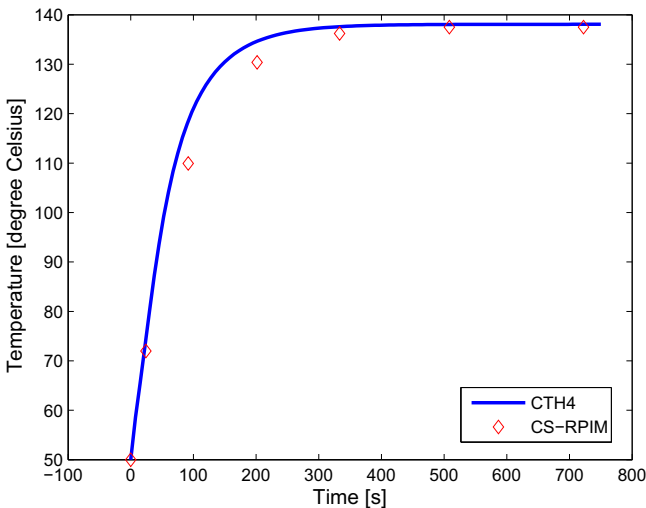


Fig. 25. Example 4.5. Evolution of temperature at point A in a square plate with a cylindrical hole.

agreement with the CS-RPIM solution [8], where the temperature at point A is found to be 137.5 °C using 354 nodes.

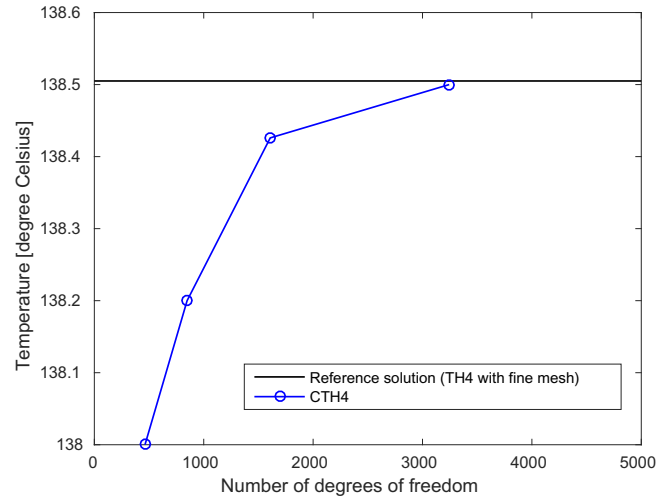


Fig. 26. Example 4.5. Convergence of temperature at point A in a square plate with a cylindrical hole.

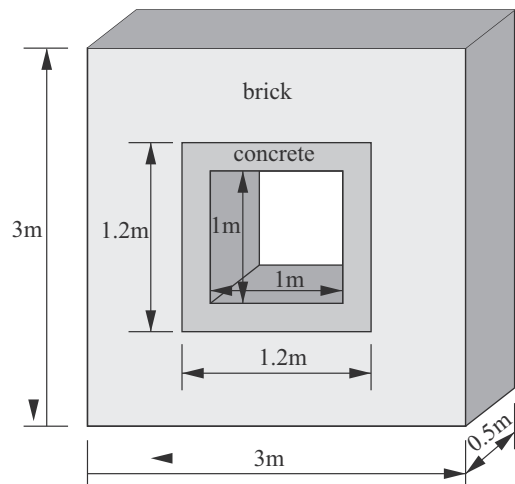


Fig. 27. Example 4.6. Geometry and parameters information of the two-walled structure.

4.6. Heat transfer in a 3D two-walled structure

The last numerical example is devoted to a more complicated domain with which the heat transfer through a section of two-walled furnace is investigated. The geometry is represented in Fig. 27 in which the inner wall is made of concrete while the outer wall is formed by brick. The conductivity of brick and concrete is set to be $k_b = 0.01$ W/mK and $k_c = 0.0057$ W/mK, respectively. A Robin-type boundary condition is imposed on the inner faces of the concrete wall to simulate how the furnace is heated from inside, where the convective coefficient is $h_{in} = 0.01$ W/m² K and the temperature in the furnace is $T_{in} = 1273$ K. The outer brick wall is in contact with ambient air at room temperature, i.e., $T_{out} = 293$ K. Heat is released through outer wall by convection, with a convective coefficient of $h_{out} = 0.068$ W/m² K. Here, the nodes on the interface between the two walls are required to recover the C⁰-continuity. A mesh of 10037 tetrahedral elements is used for the analysis (see Fig. 28).

Fig. 29 visualizes the distribution of temperature in the two-wall furnace obtained by the proposed CTH4 element, where higher value is found inside and lower is outside. Significant difference between the two limits is observed due to the low

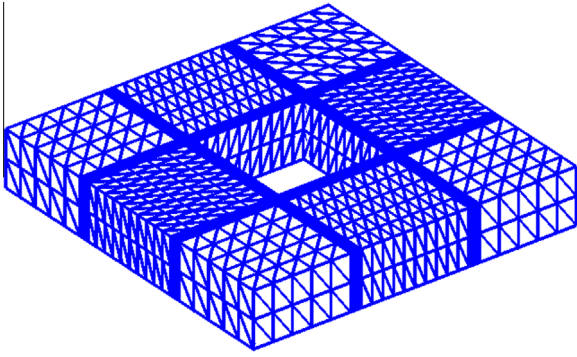


Fig. 28. Example 4.6. A finite element mesh of 10037 TH4 elements of a two-walled structure.

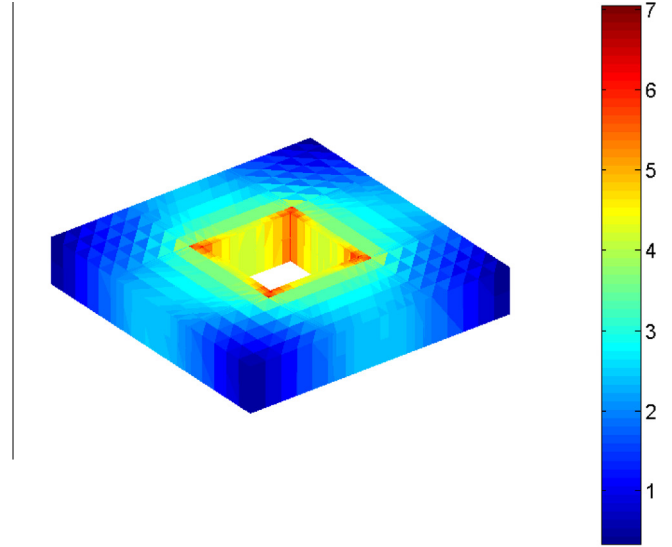


Fig. 30. Example 4.6. Comparison of the heat flux magnitude within the two-walled structure between TH4 and CTH4 elements.

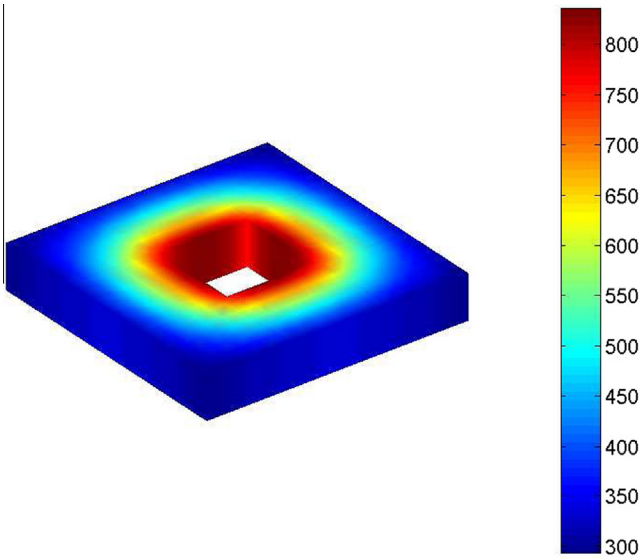


Fig. 29. Example 4.6. Temperature distribution in the two-walled structure obtained by the developed CTH4 element.

conductivity of the brick layer, which acts as heat insulation. The magnitude of the heat flux is shown in Fig. 30, demonstrating clearly the discontinuity on material interface by the conventional TH4, while it is continuous elsewhere for the CTH4 element. On the other hand, Fig. 30 also reveals one important feature that the heat flux in the whole domain obtained by TH4 elements are unsmoothed, and as expected, smoothed heat flux for the CTH4 result is found.

5. Auxiliary functions for CIP based elements: a general formulation

In this section, the derivation of a general formulation for the auxiliary functions $\phi_i, \phi_{ix}, \phi_{iy}, \phi_{iz}$ is presented, which can be used for reproducing any auxiliary functions for any types of elements in terms of the CIP method. Given a specific finite element, e.g., a 2-node line element, a 3-node triangular element, a 4-node quadrilateral element, a 4-node tetrahedral element, we denote the following terms

$$\Sigma_1 = \sum_{i=1}^n L_i, \tag{34}$$

$$\Sigma_2 = \sum_{i=1}^n L_i^2, \tag{35}$$

where n is the number of nodes within the element of interest and L_i is the Lagrangian shape function associated with the i th node of the element. The general formulation of the auxiliary functions can be written as follows:

$$\phi_i = L_i + L_i^2(\Sigma_1 - L_i) - L_i(\Sigma_2 - L_i^2), \tag{36}$$

$$\phi_{ix} = \sum_{j=1, j \neq i}^n (x_j - x_i) \left(L_i^2 L_j + \frac{1}{2} L_i L_j (\Sigma_1 - L_i - L_j) \right). \tag{37}$$

In Eq. (37), x_i and x_j denote the x -coordinate of node i and node j , respectively. The functions ϕ_{iy}, ϕ_{iz} can be obtained by replacing the x -coordinate with the y -coordinate and z -coordinate, respectively.

Next, we apply the general formulation in Eqs. (36) and (37) to reproduce the auxiliary functions for some specific elements.

For a 2-node line element, denoting the nodes as node I and node J , the auxiliary functions can be derived from the general formulation by

$$\phi_I = L_I + L_I^2 L_J - L_I L_J^2, \tag{38}$$

$$\phi_{Ix} = (x_J - x_I) (L_I^2 L_J), \tag{39}$$

$$\phi_J = L_J + L_J^2 L_I - L_J L_I^2, \tag{40}$$

$$\phi_{Jx} = (x_I - x_J) (L_J^2 L_I), \tag{41}$$

For a 3-node triangular element, we denote the three nodes as I, J and M . By using the general formulation, the auxiliary functions associated with node I presented by [9] can be reproduced exactly.

$$\phi_I = L_I + L_I^2(L_J + L_M) - L_I(L_J^2 + L_M^2), \tag{42}$$

$$\phi_{ix} = (x_j - x_i) \left(L_i^2 L_j + \frac{1}{2} L_i L_j L_M \right) + (x_M - x_i) \left(L_i^2 L_M + \frac{1}{2} L_i L_M L_j \right) \quad (43)$$

$$\phi_{iy} = (y_j - y_i) \left(L_i^2 L_j + \frac{1}{2} L_i L_j L_M \right) + (y_M - y_i) \left(L_i^2 L_M + \frac{1}{2} L_i L_M L_j \right) \quad (44)$$

Similarly, the auxiliary functions of the CIP based 4-node quadrilateral element, CQ4 element, [10] and the 4-node tetrahedral element (Eqs. (15)–(18)) can be reproduced using the general formulation proposed in Eqs. (36) and (37).

In general and in a similar manner, one can derive the auxiliary functions for any other relevant elements in the framework of the CIP method without any difficulties.

Since deriving the auxiliary functions is the key task in the application of the CIP scheme to existing finite element codes, the general formulation presented here is essential and important to the development of the proposed CIP approach. Though the above derivation has been obtained to be suitable for various element types used in 1D, 2D and 3D domains, the examination and discussion here are just some of our preliminary results, therefore a detailed and comprehensive study pertaining to this general formulation on other finite elements has to be addressed. This issue however has been scheduled for our future works.

6. Conclusions and outlook

The present work contributed to the development of alternative numerical method for heat transfer problems in 3D. The formulation of consecutive-interpolation finite element method has been for the first time extended to 3D space, leading to the introduction of the so-called *consecutive-interpolation 4-node tetrahedral element* (CTH4). In other words, a new CTH4 element in terms of CIP method has been derived. The accuracy and performance of the proposed CTh4 element is validated through a series of numerical examples with complex configurations, for the analysis of steady-state and transient heat transfer problems. In detail, the present numerical results are compared with reference solutions derived from analytical, standard finite elements, and meshless method [8]. A very good agreement among the proposed CTH4 element and other approaches is found. Some major advantages of the developed CTH4 element over the standard tetrahedral (TH4) element can be highlighted:

- Higher accuracy: given the same mesh, the CIP based elements (e.g., CTH4) results on both temperature and thermal energy (involved the calculation of temperature gradient) are shown to be higher accurate than that of the FEM (e.g., TH4).
- Higher convergence rate: CIP based elements converge to the exact solutions (i.e., analytical solution or numerical results using a fine mesh) faster than the conventional FEM.
- The nodal gradient field obtained by the CTH4 element is always smooth, while it is non-physically discontinuous is found in the conventional TH4. This smoothness is obtained by the introduction of terms related to the averaged nodal gradient into the approximation scheme, a silent feature of the present approach.
- Despite the introduction of averaged nodal gradient, the DOFs in the CTH4 still remains as the nodal temperature. Thus, the problem size does not change, leading to a conventional implementation of the present element in any existing FEM codes.
- The CTH4 shape functions possess the Kronecker-delta property, owing to the same behavior of the standard TH4 shape functions. Therefore, treating the essential boundary conditions

is made in the same way that the FEM does. This is different from meshfree methods [26,27,5] as special treatment techniques for the essential boundary conditions are required.

- When it is needed, the C^0 continuity at node can be easily recovered by a simple modification.

A useful general formulation for the auxiliary functions used in CIP scheme has been derived, which is shown to be able to reproduce exactly the auxiliary functions used for 1D element (a 2-node line element), 2D elements (a 3-node triangular element and a 4-node quadrilateral element) and a 3D four-node tetrahedral element. This provision is as preliminary results of the general formulation of auxiliary functions. It serves to assist the further development of CIP based elements. The developed CTH4 element is general and has no limitations, so in future works, it can be applied to solve other complex problems in the framework of heat transfer analysis.

Based on the results obtained and presented in Section 4, CTH4 can be considered as potential candidate or an alternative approach to the conventional FEM in solving 3D heat transfer problems. The proposed approach can be extended to model other complex problems. In terms of implementation, it is straightforward to integrate the CIP scheme into any existing FEM code. Furthermore, the numerical integration based on the Cartesian transformation method (CQT) [27] or adaptive mapping meshfree techniques [28] may be integrated into the present formulation, which is aimed to further enhance the performance of the proposed method, especially 3D problems.

Acknowledgments

Tinh Quoc Bui was supported by the Grant-in-Aid for Scientific Research – JSPS. The financial support is gratefully acknowledged. Tinh Quoc Bui is also grateful to Prof. Sohichi Hirose, Tokyo Institute of Technology, Japan for his support during the course of this work. A part of this work was supported by the Vietnam National University, Hanoi. DHD is grateful for this support.

References

- [1] H.C. Huang, A.S. Usmani (Eds.), *Finite Element Analysis for Heat Transfer: Theory and Software*, Springer-Verlag London Limited, 1994.
- [2] E. Li, Z. Zhang, Z.C. He, X. Xu, G.R. Liu, Q. Li, Smooth finite element method with exact solution in heat transfer problems, *Int. J. Heat Mass Transfer* 78 (2014) 1219–1231.
- [3] L.C. Wrobel, C.A. Brebbia (Eds.), *Boundary Element Methods in Heat Transfer*, Computational Mechanics Publications, 1992.
- [4] I. Simoes, N. Simoes, A. Tadeu, M. Reis, C.A.B. Vasoncellos, W.J. Mansur, Experimental validation of a frequency domain BEM model to study 2D and 3D heat transfer by conduction, *Elem. Anal. Boundary Elem.* 36 (11) (2012) 1686–1698.
- [5] I.V. Singh, A numerical solution of composite heat transfer problems using meshless method, *Int. J. Heat Mass Transfer* 47 (10–11) (2004) 2123–2138.
- [6] A. Singh, I.V. Singh, R. Prakash, Meshless element free Galerkin method for unsteady nonlinear heat transfer problems, *Int. J. Heat Mass Transfer* 50 (5–6) (2007) 1212–1219.
- [7] L.H. Liu, J.Y. Tan, Meshless local Petrov–Galerkin approach for coupled radiative and conductive heat transfer, *Int. J. Therm. Sci.* 46 (2007) 672–681.
- [8] X.Y. Cui, S.Z. Feng, G.Y. Li, A cell-based smoothed radial point interpolation method (CS-RPIM) for heat transfer analysis, *Eng. Anal. Boundary Elem.* 40 (2014) 147–153.
- [9] C. Zheng, S.C. Wu, X.H. Tang, J.H. Zhang, A novel twice-interpolation finite element method for solid mechanics problems, *Acta Mech. Sinica* 26 (2) (2010) 265–278.
- [10] T.Q. Bui, D.Q. Vo, C. Zhang, A consecutive-interpolation quadrilateral element (CQ4): Formulation and applications, *Finite Elements Anal. Des.* 84 (2014) 14–31.
- [11] T.Q. Bui, D.D. Nguyen, X.D. Zhang, S. Hirose, R.C. Batra, Analysis of 2-dimensional transient problems for linear elastic and piezoelectric structures using the consecutive-interpolation quadrilateral element (CQ4), *Eur. J. Mech. A/Solids* 58 (2016) 112–130.

- [12] Z. Kang, T.Q. Bui, D.D. Nguyen, T. Saitoh, S. Hirose, An extended consecutive-interpolation quadrilateral element (XCQ4) applied to linear elastic fracture mechanics, *Acta Mech.* 226 (12) (2015) 3991–4015.
- [13] I. Keles, C. Conker, Transient hyperbolic heat conduction in thick-walled cylinders with exponentially-varying properties, *Eur. J. Mech.* 30 (2011) 449–455.
- [14] H.-J. Jiang, H.L. Dai, Analytical solutions for three-dimensional steady and transient conduction problems of a double-layer plate with a local heat source, *Int. J. Heat Mass Transfer* 89 (2015) 652–666.
- [15] E.O. Reséndiz-Flores, I.D. García-Calvillo, Numerical solution of 3D non-stationary heat conduction problems using the Finite Pointset Method, *Int. J. Heat Mass Transfer* 87 (2015) 104–110.
- [16] A. Tadeu, J. Prata, N. Simoes, Dynamic simulation of three-dimensional heat conduction through cylindrical inclusions using a BEM model formulated in the frequency domain, *Appl. Math. Comput.* 261 (2015) 397–407.
- [17] S.Z.F.X.Y. Cui, A.M. Li, G.Z. Xie, A face-bases smoothed point interpolation method (FS-PIM) for analysis of nonlinear heat conduction in multi-material bodies, *Int. J. Therm. Sci.* 100 (2016) 430–437.
- [18] W. Chen, G. Pang, A new definition of fractional laplacian for modeling three-dimensional non-local heat conduction, *J. Comput. Phys.* (2016), <http://dx.doi.org/10.1016/j.jcp.2016.01.003>.
- [19] S. Gerace, K. Erhart, A. Kassab, E. Divo, A model-integrated localized collocation meshless method for large scale three-dimensional heat transfer problems, *Eng. Anal. Boundary Elem.* 45 (2012) 2–19.
- [20] M. Shibahara, S.N. Atluri, The meshless local Petrov–Galerkin method for the analysis of heat conduction due to a moving heat source, in welding, *Int. J. Therm. Sci.* 50 (2011) 984–992.
- [21] S.C. Wu, X. Peng, W.H. Zhang, S.P.A. Bordas, The virtual node polygonal element method for nonlinear thermal analysis with application to hybrid laser welding, *Int. J. Heat Mass Transfer* 67 (2013) 1247–1254.
- [22] S.K. Dubey, P. Srinivasan, Development of three-dimensional transient numerical heat conduction model with growth of oxide scale for steel billet reheat simulation, *Int. J. Therm. Sci.* 84 (2014) 214–227.
- [23] M. Allahbakhshi, M. Akbari, Heat analysis of the power transformer bushings using the finite element method, *Appl. Therm. Eng.* (2016), <http://dx.doi.org/10.1016/j.applthermaleng.2016.02.065>.
- [24] J.P. Holman, *Heat Transfer*, tenth ed., McGraw-Hill, 2010.
- [25] B. Dai, B. Zheng, L. Wang, Numerical solution of transient heat conduction problems using improved meshless local Petrov–Galerkin method, *Appl. Math. Comput.* 219 (2013) 10044–10052.
- [26] T.Q. Bui, M.N. Nguyen, C. Zhang, An efficient meshfree method for vibration analysis of laminated composite plates, *Comput. Mech.* 48 (2) (2011) 175–193.
- [27] T.Q. Bui, A. Khosravifard, C. Zhang, M.R. Hematiyan, M.V. Golub, Dynamic analysis of sandwich beams with functionally graded core using a truly meshfree radial point interpolation method, *Eng. Struct.* 47 (2013) 90–104.
- [28] D. Racz, T.Q. Bui, Novel adaptive meshfree integration techniques in meshless methods, *Int. J. Numer. Methods Engng.* 90 (2012) 1414–1434.